Indian Journal of Chemistry
Vol. 60A April 2021, pp. 545-555

Structure and electronic properties of mono and di-methyl substituted poly(*p*-phenylenebenzobisthiazole) oligomers: A computational study

J Laxmikanth Rao*

Department of Catalysis and Fine Chemicals, CSIR-Indian Institute of Chemical Technology, Hyderabad 500 007, India

*E-mail:lkjoshi@iict.res.in

Received 23 November 2020; revised and accepted 15 February 2021

The structural and electronic properties of mono and di-methyl substituted poly(*p*-phenylene benzobisthiazole) oligomers have been investigated theoretically employing quantum chemical calculations based on density functional theory (DFT) using the B3LYP functional. The neutral states geometries of these oligomers have been used to calculate the HOMO-LUMO gaps (Δ_{H-L}), ionization potentials (IP) and electron affinities (EA). The lowest excitation energies (E_g) and the maximum absorption spectra have been studied using the TDDFT/B3LYP/6-31G(D) method. The cationic and anionic states of these oligomers have been optimized using the same methodology. The optimized lowest singlet excited-state geometries of oligomers have been used to calculate the emission spectra by using TDDFT method. The Δ_{H-L}s, IPs, EAs, E_gs, and absorption/emission spectra of the respective polymer have been obtained by extrapolating those of the oligomers to the inverse chain length equal to zero. From the reorganization energies, it can be seen that the electron transport energy values are smaller than the hole transport suggesting that these could be used as electron transport materials in light emitting diodes devices. Thus, these studies on the oligomers will help in rationalizing the properties of known polymers and to predict those of yet unknown ones for their utilization in electronic devices.

Keywords: Benzobisthiazole, TDDFT, Oligomer, Homo-Lumo gap, Reorganization energy

During the past few decades, the conjugated polymers[1] have been the focus of research interest for both the scientific and technological community because of their potential application in solar cells[2], organic transistors[3], nonlinear optical devices and light emitting diodes (LED)[4]. In recent years particularly the interest has been grown in electronic devices, which are fabricated from the conjugated polymers and are well suited for flat panel displays due to their fast response times, good processability, low-operating voltages and excellent colour gamut[5]. Since the first discovery of electroluminescence material from poly(*p*-phenylenevinylene) (PPV)[1], a tremendous effort has been made towards the development of conjugated polymers as light emitting materials. Until now a wide range of conjugated polymer systems including PPV, poly(*p*-phenylene)[6], polyfluorene[7], polythiophene[8] and polycarbozoles[9] and some copolymers[10] have been investigated as active materials in LEDs.

Investigation and synthesis of new conjugated polymers have become essential to improve the electronic and optoelectronic properties of these materials, which in turn improves the device performance. In addition to this, the achievement of high electron affinity (EA) conjugated polymers (for electron injection/transport) and low ionization potential conjugated polymers (for hole injection/ transport), which are desirable in the polymer electronic devices pose a great challenge. Thus, one can modify the EAs and ionization potentials (IPs) of these conjugated polymers by the introduction of electron-donating/ withdrawing groups to the parent moiety[11]. For the last two decades poly(*p*-phenylenebenzobisthiazole) (PBZT), which is one of the high-performance rigid-rod polymers, have drawn attention, because of its excellent mechanical as well as thermal properties and environmental stabilities[12,13]. Such exceptional properties originate from its unique rigid backbone molecular structure consisting of benzobisthiazole and phenyl rings. The polymer is a rigid-rod polymer because the molecules are collinearly arranged and have rotational flexibility in the backbone only at the heterocyclic and phenyl ring linkages. It has been suggested that flexibility can also be enhanced by the introduction of side chains[14]. The extended chain in the polymer, which also allows delocalization of the π-electrons along the polymer backbone, could play a key role in determining the properties related to structural, optical and electrical properties[15-17].

Quantum chemical studies on the electronic structure properties of known polymers have contributed a lot to rationalize their properties and successfully used to predict those of yet unknown one[18,19]. To evaluate the electronic structure properties of polymers, two different theoretical approaches are used. One is the polymer approach, in which the periodic structures are assumed for infinite polymers[20]. The other one which is gaining popularity presently is the oligomer extrapolation technique, in which a sequence of increasing chain length oligomer properties are calculated and extrapolated to infinite chain length. A distinct advantage of this technique is that it provides the convergence behaviour of the structural, electronic and optical properties of polymers and this has been successfully applied to investigate several types of oligomers for their structure property relationships[18,21-23]. Thus, knowledge of the oligomer structure-property relationship helps design the polymer, thereby one can achieve material's explicit property. In the present study, this technique is applied to gain a more comprehensive understanding regarding the effect of conjugation and effect of orientation of donor substitution on IPs, EAs and the reorganization energies (for hole/electron transport) for some methyl donor substituted PBZTs using density functional theory (DFT) calculations and to explore the possibility to utilize them in LED devices.

Materials and Methods

Computational methodology

The ground state geometries of all these oligomers have been optimized using DFT at the B3LYP/6-31G(D) level, using G09W package[24]. Conformational analysis has been carried out by considering the monomer unit of the oligomers using same methodology. To study the charge transfer and absorption properties, TDDFT calculations have been carried out by considering the DFT/B3LYP/6-31G(D) optimized geometries of all these oligomers and are compared with the available experimental data. The excited state geometries of the oligomers are optimized by CIS/6-31G(D) and the emission spectra have been calculated by using TDDFT method[24]. To calculate IP, EA, extraction potential and reorganization energies, the energies of the cation and anions of these oligomers are necessary. For this purpose, the open shell optimizations have been carried out on both the cation and anions of these oligomers using the UB3LYP/6-31G(D) methodology[24]. To get the polymeric information, the linear extrapolation technique has been used, in this, the the Δ_{H-L}, IP, EA, HEP and EEPs of the oligomers have been extrapolated to the infinite chain length (i.e.,1/n=0)[20-23].

Results and Discussion

Conformational analysis

The ground state potential energy curve around the (methyl substituted) phenyl ring (P) and the benzobisthazole moiety (B) is obtained by considering the monomer unit of all the oligomers. The torsion angle between the P-ring and the B-moiety is constrained in 10° increments (0°- 180°), followed by optimizing all remaining parameters using DFT/B3LYP/6-31G(D) method. The potential energy curve is obtained by plotting the torsional potentials (which could be obtained by subtracting the energy of the optimized monomer structure from the torsion constrained monomer energy) as a function of torsion angle between the P and B (Fig. 1). It can be seen that the potential energy curve is virtually identical for both the Me-PBZT and di-Me-PBZT, when compared to the unsubstituted PBZT. The methyl substitution(s) lowers the energy barrier, when compared to the unsubstituted PBZT, similar theoretical results have been obtained previously by using such model compounds. Here the energy barriers to phenyl rotations are calculated as 5.41, 3.67 and 3.54 Kcal/mol for the unsubstituted PBZT, Me-PBZT,

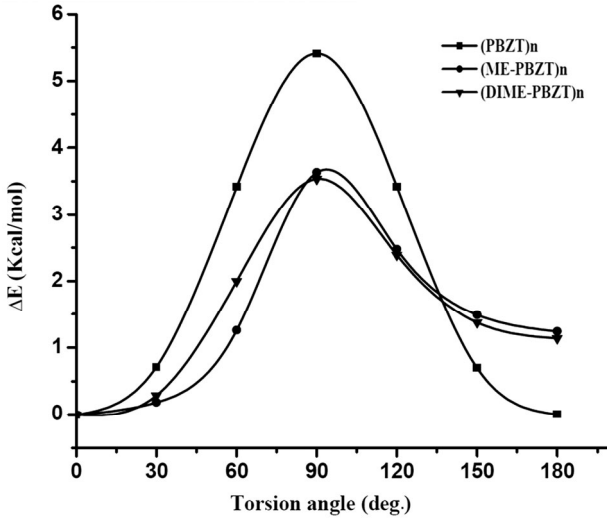

Fig. 1 — Torsional potential energy curves for monomers of PBZT, Me-PBZT, and di-Me-PBZT obtained by B3LYP/6-31G(D) method

di–Me-PBZT, respectively, which are in good agreement with the previously reported values[25-28].

Structural properties of ground states

The sketch map of the structures namely poly(*p*-phenylenebenzobisthiazole) $(PBZT)_n$, poly(methyl-*p*-phenylenebenzobisthiazole) $(Me\text{-}PBZT)_n$, and poly(di-methyl-*p*-phenylenebenzobis-thiazole) $(di\text{-}Me\text{-}PBZT)_n$, (n=1-4) are shown in Fig. 2. The optimized structures of $(PBZT)_4$, $(Me\text{-}PBZT)_4$, and $(di\text{-}Me\text{-}PBZT)_4$ by DFT/B3LYP/6-31G(D) are shown in Fig. 3. These oligomers are optimized using DFT/B3LYP/6-31G(D) method without imposing any geometrical constraints. The important inter-ring bond length and dihedral angles along with dipole moment of the neutral ground states are shown in Supplementary Data, Table S1 and it can be seen that the inter-ring bond lengths between the P and B-moiety do not vary appreciably with the oligomer size, but the dihedral angles between the P and B, especially in case of the $(Me\text{-}PBZT)_n$ $(di\text{-}Me\text{-}PBZT)_n$ gradually changes as the oligomer size increases (Supplementary Data, Table S1). This increase may be due to the steric hindrance between the N-atom of the B-moiety and the methyl group(s) present on the phenyl rings. The optimized unsubstituted PBZT oligomers are found to be planar having zero dihedral angle between the P-ring and B-moiety. From the X-ray structure analysis, the dihedral angle between the P and B is found to be 20.5° for the unsubstituted PBZT[29]. In the case of the $(PBZT)_n$ oligomers, during the calculation it is seen that only a small energy difference is observed from rotating the phenyl ring from the optimal *ab initio* value to the experimental value, which is in agreement with the previous report[25-28].

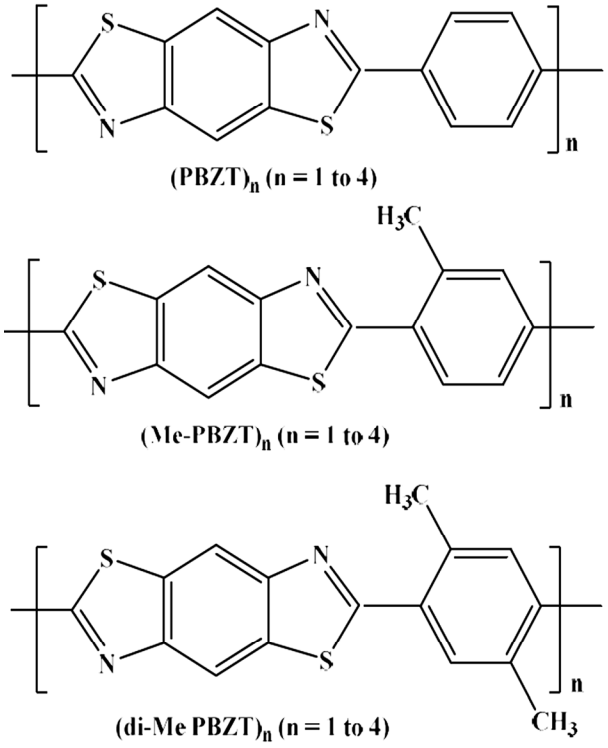

Fig. 2 — The sketch map of the oligmers considered for this study

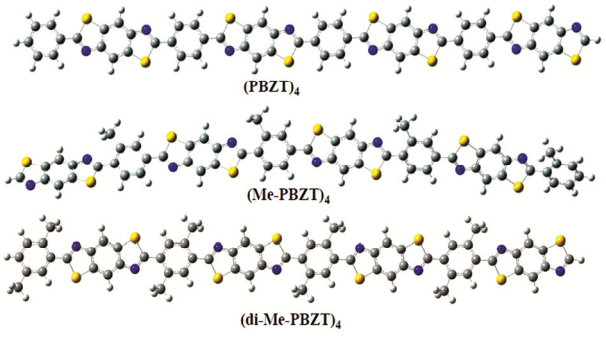

Fig. 3 — Optimized geometries for $(PBZT)_4$, $(Me\text{-}PBZT)_4$, and $(di\text{-}Me\text{-}PBZT)_4$ obtained by B3LYP/6-31G(D) method

In case of $(Me\text{-}PBZT)_n$ and $(di\text{-}Me\text{-}PBZT)_n$ the dihedral angle between the B and P varies from ~20 – 25° and ~21 – 25°, respectively, whereas the dihedral angle between the P and B for these oligomers varies from ~1 – 3° and ~21 – 23°, respectively. The increase in the dihedral angle between the P and B in the $(di\text{-}me\text{-}PBZT)_n$ may be due to the presence of steric repulsions between the N-atom of the thiazole unit and the methyl substitutions on the phenyl ring[27]. It is observed that generally, the dipole moments tend to increase with increasing oligomeric size in all series (Supplementary Data, Table S1). This may be due to an increase in conjugation. Thus, these results suggest that we can approximately describe the basic structure of the polymers as their oligomers.

Frontier molecular orbitals

It will be useful to examine the frontier molecular orbitals i.e., highest occupied molecular orbitals (HOMO) and the lowest unoccupied molecular orbitals (LUMO) of these oligomers because the relative ordering of these orbitals provides a reasonable qualitative indication of the excitation properties and the ability to electron transport or hole transport. The electronic density contours of the frontier orbitals i.e., HOMO and LUMOs of $(PBZT)_n$, $(Me\text{-}PBZT)_n$, and $(di\text{-}Me\text{-}PBZT)_n$ (n=1, 4), obtained by B3LYP/6-31G(D) method are shown in Fig. 4. It can be seen that generally in all the oligomers studied here, the frontier molecular orbitals are spread over

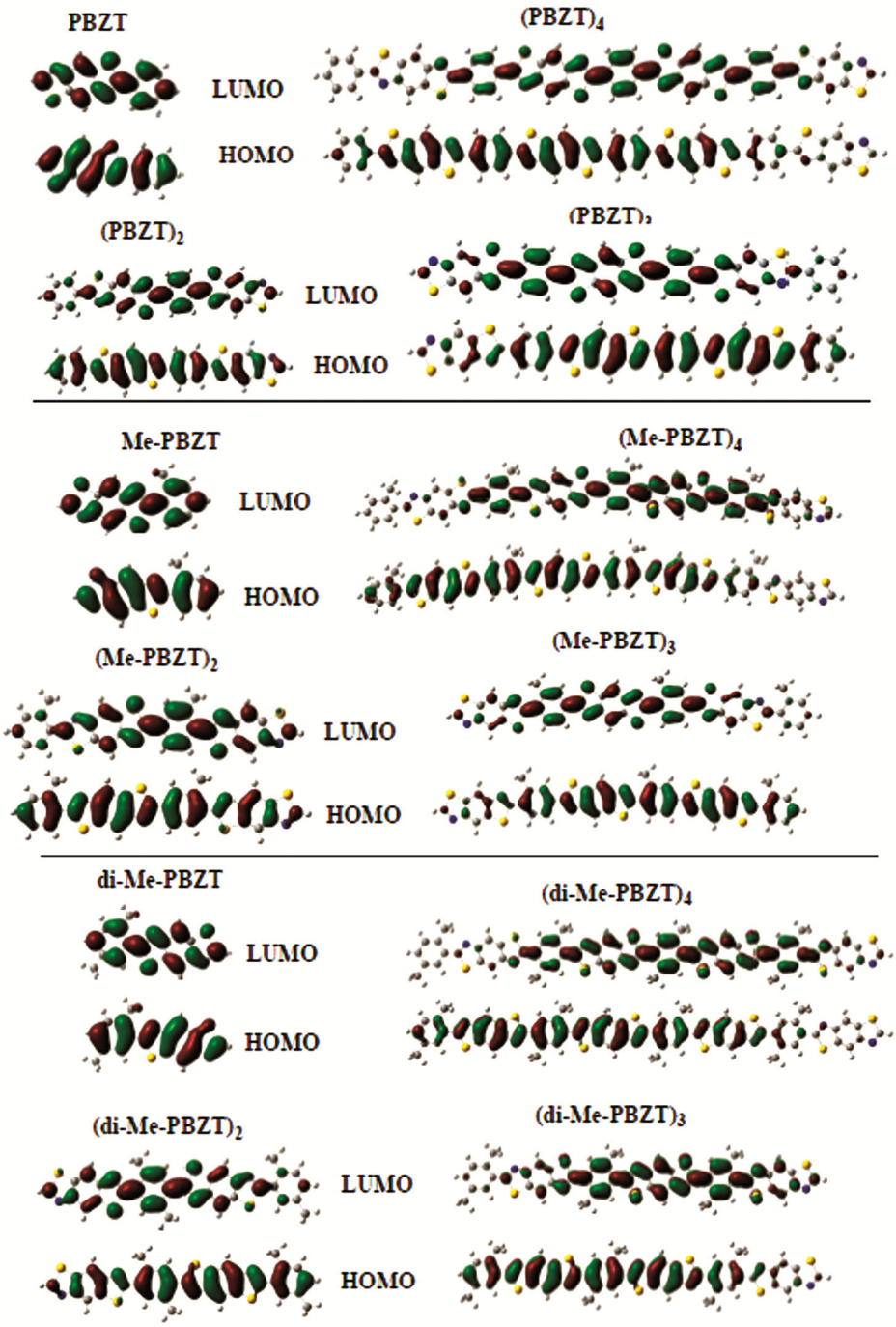

Fig. 4 — The contour plots of HOMO and LUMO orbitals of $(PBZT)_n$, $(Me\text{-}PBZT)_n$, and $(di\text{-}Me\text{-}PBZT)_n$ (n=1–4) (from top to bottom) obtained by B3LYP/6-31G(D) method

the whole π-conjugated backbone, although the largest contributions come from the different parts of the chromophores. It is seen that in HOMOs, there is inter-ring antibonding between the bridge atoms, and there is intra-ring bonding between the bridge carbon atoms and its conjoined atoms. On the contrary, in the LUMO, there is inter-ring bonding between the bridge single bond and intra-ring antibonding between the bridging atom and its neighbour. In general, the HOMO possesses antibonding character between the subunits of the oligomers and which may explain the nonplanarity observed for these oligomers in their

ground states. On the other, hand the LUMO of all the oligomers generally shows bonding character between the two adjacent subunits. This implies that the singlet excited state should be more planar, involving mainly the promotion of an electron from the HOMO to the LUMO. It is observed that in all the oligomers, the localization of the electronic cloud distribution is in the middle part of the oligomer, which may be due to the chain-end effects (Fig. 4)[30]. In contrast, asymmetric electronic cloud character prevails in both the HOMO and LUMO when the methyl groups are substituted on the phenyl ring in different positions. The HOMO remains delocalized on the right parts of the conjugated backbone whereas the LUMO on the left parts. This may be due to the electron donating property of the methyl substituted phenyl and the electron withdrawing nature of the B-moiety.

In the experiment, the HOMO and LUMO energies are calculated from the empirical formula based on the onset of the oxidation and reduction peaks measured by cyclic voltammetry, assuming the absolute energy level of ferrocene/ferrocenium to be 4.8 eV below vacuum[17]. In the present study, the HOMO and LUMO energies are calculated using DFT/B3LYP/6-31G(D) method and are tabulated in Table 1. In this method, solid-state packing effects are not included, which tends to significantly reduce the torsion angle between the adjacent units and thereby affects the HOMO and LUMO energy levels in a thin film when compared to an isolated molecule. Even though these calculated, energies are not accurate but are useful in acquiring information about these energies by comparing similar oligomers and polymers. The HOMO and LUMO energies of these oligomers are plotted as a function of the inverse number of monomer units (Fig. 5) to get the information about the polymer. As expected in the π-conjugated systems, the energy of the frontier orbital levels evolves linearly with the inverse chain length in all the systems i.e., HOMO energies increases, whereas the LUMO energies decrease[31].

It is seen from Table 1 and Fig. 5, that the introduction of electron donating group i.e., methyl groups(s) on the phenyl ring slightly lifts the HOMO of the longest oligomer of Me-PBZT and di-Me-PBZT by ~ 0.036 eV and 0.005 eV, respectively, when compared to the unsubstituted PBZT (-5.698 eV). In the case of the LUMO levels of the oligomers, the energies of Me-PBZT (-2.590 eV), and di-Me-PBZT (-2.497 eV) are stabilized by 0.081 and 0.174 eV, respectively, with respect to the unsubstituted PBZT (-2.671 eV). Since the HOMO shows inter-ring antibonding character and the LUMO shows inter-ring bonding character, the variation of dihedral angles between the subunits should have some effect on LUMO. In the case of substituted-PBZT, the LUMO energy levels are decreased when compared to the unsubstituted PBZT. This may be attributed to the

Table 1 — The negative HOMO (ε_{HOMO}) , LUMO (ε_{LUMO}) energies and HOMO–LUMO gaps (Δ_{H-L}) obtained by B3LYP/ 6-31G(D) and the lowest excitation energies (E_g (TD)) obtained by TDDFT/ B3LYP/6-31 G(D) for all the oligomers

	$-\varepsilon_{HOMO}$ (eV)	$-\varepsilon_{Lumo}$ (eV)	Δ_{H-L} (eV)	E_g-TD (eV)
$(PBZT)_n$				
n=1	6.046	1.868	4.178	3.791
n=2	5.800	2.442	3.358	3.035
n=3	5.726	2.600	3.126	2.773
n=4	5.698	2.671	3.027	2.663
n=∞	5.572	2.959	2.613	2.328
Expt.			2.480[a]	
$(Me\text{-}PBZT)_n$				
n=1	6.065	1.780	4.286	3.789
n=2	5.807	2.363	3.444	3.033
n=3	5.730	2.518	3.212	2.774
n=4	5.703	2.585	3.118	2.734
n=∞	5.571	2.878	2.692	2.373
$(di\text{-}Me\text{-}PBZT)_n$				
n=1	6.009	1.743	4.266	3.789
n=2	5.782	2.280	3.502	3.033
n=3	5.718	2.431	3.287	2.774
n=4	5.694	2.497	3.196	2.665
n=∞	5.578	2.767	2.811	2.519

[a]see ref. 33

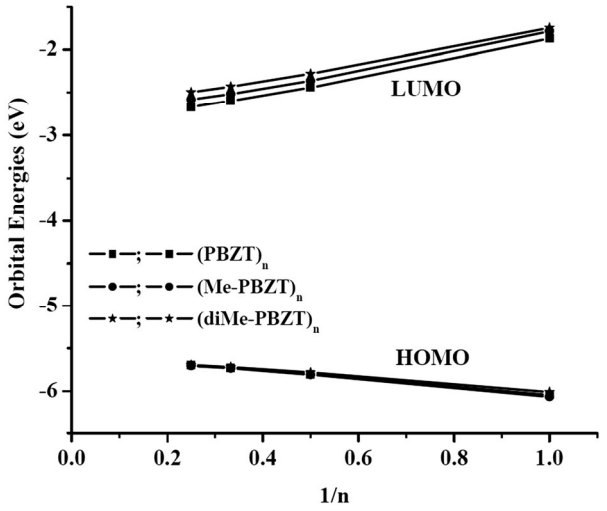

Fig. 5 — Calculated HOMO and LUMO energies of all the oligomers as a function of the inverse number of monomer units using B3LYP/6-31G(D) method

electron conjugation spread over the whole molecule and thus stabilize the LUMO levels.

Structural properties of the ionic states

One of the most important features of the π-conjugated polymers is their ability to become highly conducting after reductive (n-type) and oxidative (p-type) doping[17]. Hence the cationic and anionic geometry optimization of all the oligomers is carried out by using DFT/UB3LYP/6-31G(D) method. The important inter-ring bond lengths and dihedral angles for the optimized cationic and anionic geometries of all the oligomers are tabulated in Supplementary Data, Table S2 and S3, respectively. It can be seen from that the geometry deformations of the positively and negatively charged oligomers are found to be evenly spread over the entire chain, which indicates that no self-localized polaron is formed. This is analogous to the earlier DFT results obtained for positively and negatively charged oligomers[17].

It can be seen that the inter-ring distances between the two adjacent units decrease in both the cationic and anionic states in all oligomers when compared to their neutral states (Supplementary Data, Table S1-S3). This may be due to the addition of an electron or a hole to the oligomer, which decreases the inter-ring distance in ionic states relative to the neutral state and can be explained by considering the frontier molecular orbitals i.e., HOMO and LUMOs. From Fig. 4, it can be seen that in HOMOs of all the oligomers, there is inter-ring antibonding between the bridge atoms, and there is intra-ring bonding between the bridge carbon atoms and its conjoined atoms. Hence, the removal of an electron from HOMO leads to shortening of the inter-ring bond distance in the cationic state relative to the neutral state. On the other hand, the LUMO of all the oligomers generally shows bonding character between the two adjacent moieties. The shortening of the inter-ring bond distance in the anionic state due to the bonding interactions occurring between the π-orbitals on the two adjacent (methyl substituted) phenyl rings and the benzobisthiazole moieties. The injection of electrons and holes in these oligomers induces conjugation than their corresponding neutral states, which results in decreasing the dihedral angles between the subunits of each oligomer in cationic and anionic states when compared with their corresponding neutral states. In the anionic states of these oligomers, the inter-ring dihedral angles are even smaller when compared with the corresponding cationic states, indicating that the whole molecule tends to be more planar with the injection of electrons or holes in these oligomers.

Ionization potentials and electron affinities

The IPs and EAs are useful in estimating the energy barrier for the injection of holes/electrons into the polymer. The adequate and balance transport of both injected electron and holes plays a crucial role in optimizing the performance of LED devices. The vertical IP/EA (IP_V/EA_V: the difference between the energy of cationic/anion and neutral states in the optimized geometry for the neutral state) and adiabatic IP/EA (IP_a/EA_a: the difference between the energy of cationic/anionic optimized geometry and neutral optimized geometry states) are calculated and tabulated in Table 2. To get the polymeric information, we have extrapolated the IP_V/EA_V and IP_a/EA_a values to the infinite chain length ($n=\infty$) for all the oligomers and all the data show excellent linearity in all the oligomers. The energy required to create a hole in the polymer varies from 5.909 to 6.093 eV and the extraction of an electron from the anion varies from 2.246 to 2.425 eV, depending on the orientation of the methyl substitution in the polymer.

HOMO-LUMO gaps

It is well known that the energy gap of the polymer $(M)_n$ is the difference between the HOMO and LUMO

Table 2 — Ionization Potentials (IPs) and electron affinities (EAs) of all the oligomers

	IP_V (eV)	IP_a (eV)	EA_V (eV)	EA_a (eV)
$(PBZT)_n$				
n=1	7.528	7.360	-0.432	-0.581
n=2	6.839	6.729	-1.387	-1.509
n=3	6.555	6.479	-1.753	-1.839
n=4	6.394	6.336	-1.954	-2.018
n=∞	6.093	6.017	-2.246	-2.455
$(Me\text{-}PBZT)_n$				
n=1	7.750	7.671	-0.428	-0.576
n=2	6.801	6.693	-1.371	-1.495
n=3	6.520	6.443	-1.729	-1.822
n=4	6.393	6.323	-1.886	-1.972
n=∞	5.909	5.847	-2.390	-2.424
$(di\text{-}Me\text{-}PBZT)_n$				
n=1	7.414	7.259	-0.401	-0.552
n=2	6.743	6.642	-1.348	-1.469
n=3	6.528	6.425	-1.603	-1.761
n=4	6.372	6.296	-1.797	-1.925
n=∞	6.061	5.985	-2.425	-2.369

energies when n =∝, termed as HOMO-LUMO gaps (Δ_{H-L}). However, it is difficult to obtain the correct data by experiment due to the experimental restrictions such as interchain interactions, solvent effects, and so on. The experimental energy gap is usually observed by two methods: the maximal wavelength in the absorption spectra from ultraviolet light or cyclic voltammograms (CV)[32]. These methods are valid only when the lowest singlet excited state can be described by only one singly excited configuration, in which an electron is promoted from HOMO to LUMO; in such a condition the experimental restrictions, can be neglected. Theoretically, there are two ways to estimate the energy gap namely from the HOMO-LUMO gaps and the other from the lowest excitation energies (E_g) of the oligomers. In the present study, the Δ_{H-L} and (E_g(TD)) are obtained from DFT/B3LYP/6-31G(D) and TDDFT/B3LYP/6-31G(D) methods, respectively, and the results are shown in Table 1. The above energies for infinite polymeric chains are determined by plotting these values against the reciprocal of the number of monomer units and by extrapolating to infinity (Supplementary Data, Figs S1 and S2, respectively).

It is seen from Table 1, in the case of $(PBZT)_n$ there is a good agreement between the calculated HOMO-LUMO gap using the DFT method and the experiment[33]. The calculated optical band gap for $(PBZT)_n$ polymer differs by 0.15 eV from the experimentally observed one i.e., 2.48 eV [16,33]. It is seen that the TDDFT method underestimates the energy gap for the same polymer. This may due to i) the limitation of the current approximate exchange-correlation functionals, which are used in describing the exchange-correlation potentials in the asymptotic region[34]; ii) the calculations are carried out for the isolated gas-phase oligomers, whereas the experimental band gaps are measured in the liquid phase in which environmental influences may be involved; iii) presence of intermolecular packing forces[35].

Absorption spectra

The study the absorption properties, TDDFT calculations have been carried out by considering the DFT/B3LYP/6-31G(D) optimized geometries of all these oligomers and are compared with the available experimental data (Table 3). It can be seen from the Table 3, generally, all the electronic transitions are of π–π* type and involve both subunits of the molecule and no localized electronic transitions are observed among the first five singlet-singlet transitions. In each oligomer, the lowest lying singlet excited state S_1, which is optically allowed and corresponds to the promotion of an electron from the HOMO to the LUMO. Furthermore, the oscillator strength of the lowest π–π* singlet excited state to the ground state, increases strongly when going from an isolated molecule to an oligomer. The oscillator strength associated with the S_1 state increases approximately one order of magnitude upon adding one repeating unit to the monomer in all the oligomers studied here. As the strongest absorption peaks in all these oligomers are assigned to π–π* electronic transition, arising exclusively from $S_0 \rightarrow S_1$ electronic transition which is mainly composed of HOMO→LUMO transition. It can be seen in all the series of these oligomers, as the conjugation length increases, the absorption wavelength also increases progressively, thereby the HOMO–LUMO gaps decrease accordingly. It can be seen that in the case of unsubstituted PBZT, there is good agreement between the experimentally observed absorption i.e., 468 nm[16,33] and the TDDFT calculated absorption i.e., 466 nm. It can also be seen that the mono methyl substitution shifts the absorption by ~10nm (453 nm) when compared to the unsubstituted $(PBZT)_4$ (~468 nm) and the di methyl substitution still shifts the absorption by another ~10nm (i.e., 441 nm). Due to the lack of experimental data, we are unable to

Table 3 — Electronic transitions data obtained by the TDDFT/B3LYP/6-31G(D) for all the oligomers

		Major contributions	λ_{max} (nm)	*f*
PBZT	$S_0 \rightarrow S_1$	H→ L (60%)	316	0.8014
$(PBZT)_2$	$S_0 \rightarrow S_1$	H→ L (88%)	409	2.1680
$(PBZT)_3$	$S_0 \rightarrow S_1$	H→ L (88%)	447	3.4211
$(PBZT)_4$	$S_0 \rightarrow S_1$	H→ L (84%)	466	4.6799
Expt.			468[a]; 467[b]	
Me PBZT	$S_0 \rightarrow S_1$	H→ L (80%)	318	0.8200
$(Me\text{-}PBZT)_2$	$S_0 \rightarrow S_1$	H→ L (88%)	409	2.1625
$(Me\text{-}PBZT)_3$	$S_0 \rightarrow S_1$	H→ L (88%)	447	3.4122
$(Me\text{-}PBZT)_4$	$S_0 \rightarrow S_1$	H→ L (83%)	453	4.5643
di-Me-PBZT	$S_0 \rightarrow S_1$	H→ L (87%)	320	0.8009
$(di\text{-}Me\text{-}PBZT)_2$	$S_0 \rightarrow S_1$	H→ L (88%)	410	2.1397
$(di\text{-}Me\text{-}PBZT)_3$	$S_0 \rightarrow S_1$	H→ L (87%)	426	3.2512
$(di\text{-}Me\text{-}PBZT)_4$	$S_0 \rightarrow S_1$	H→ L (80%)	441	4.5060

[a] see ref. 33; [b] see ref. 16.

compare the calculated absorption values of methyl substituted oligomers with the experiment.

Properties of excited structures and emission spectra

The standard procedure adopted for calculating excited-state properties of larger molecules is the configuration interaction singles (CIS) method. These results are useful in acquiring information regarding the excited states. The excited state optimizations have been carried out on all the oligomers using CIS/6-31G(D) method. For the sake of brevity, the optimized excited state geometries of dimers of PBZT, me-PBZT, and di-me-PBZT only are shown in Fig. 6, along with corresponding HF/6-31G(D) optimized geometries. It is seen that the main character of the frontier molecular orbitals obtained by this method is similar to the frontier molecular orbitals obtained by B3LYP/6-31G(D) method. It can be seen from the Fig. 6, in the ground (S_0) and lowest singlet excited states (S_1), some of the bond lengths are lengthened and some are shortened. These differences in the bond lengths can be predicted from their frontier molecular orbital nodal patterns because the lowest singlet state corresponds to excitation from HOMO to LUMO in all of these oligomers studied here. We can explore the bond length variation by analyzing the HOMO and LUMOs. It can be seen from Fig. 6, in case of $(PBZT)_2$, the HOMO has bonding across the r(1,5), r(3,4), r(4,9), r(6,7), r(7,8), r(10,11), r(13,14), r(13,18), r(15,16), r(16,17), r(19,23), r(21,22), r(22,25), r(24,26), r(26,30), r(27,28), r(31,32), r(31,36), r(33,34) and r(34,35), but the LUMO has nodes in these regions. Therefore, one can expect elongation of these bonds and the data in the Fig. 6 show that these bonds are considerably longer in the excited state. The HOMO has a node across the r(4,5), r(3,6), r(8,9), r(7,10), r(11,13), r(14,15), r(18,17), r(16,19), r(21,24), r(22,23), r(25,30), r(26,27), r(29,31), r(32,33) and r(35,36) bonds in $(PBZT)_2$, while the LUMO shows bonding in these regions. Thus the data confirm the anticipated contraction of these bonds. A similar trend is observed in all these remaining dimers. The dihedral angles ϕ(10,11,13,14), ϕ(15,16,19,20) and ϕ(27,28,31,32) in case of $(di\text{-}me\text{-}PBZT)_2$ reduced from 38.2°, 38.6° and 38.8° obtained by HF/6-31G(D) to nearly 0.0°, 0.0° and 24.8° obtained by CIS/6-31G(D) method respectively, implying that the bonds r(11,13), r(16,19) and r(28,31) rotates during excitation. No such significant trend is observed in the case of other oligomers. It is clear from these results that the excited structure has a strong coplanar nature which indicates that the conjugation is better in the excited structure, which is consistent with the estimation from the character of the frontier orbitals.

For the emission spectra, the TDDFT calculations have been carried out using the first excited state geometries which are optimized by the CIS/6-31G(D) method. The transition energies and major configuration along with their oscillator strengths are

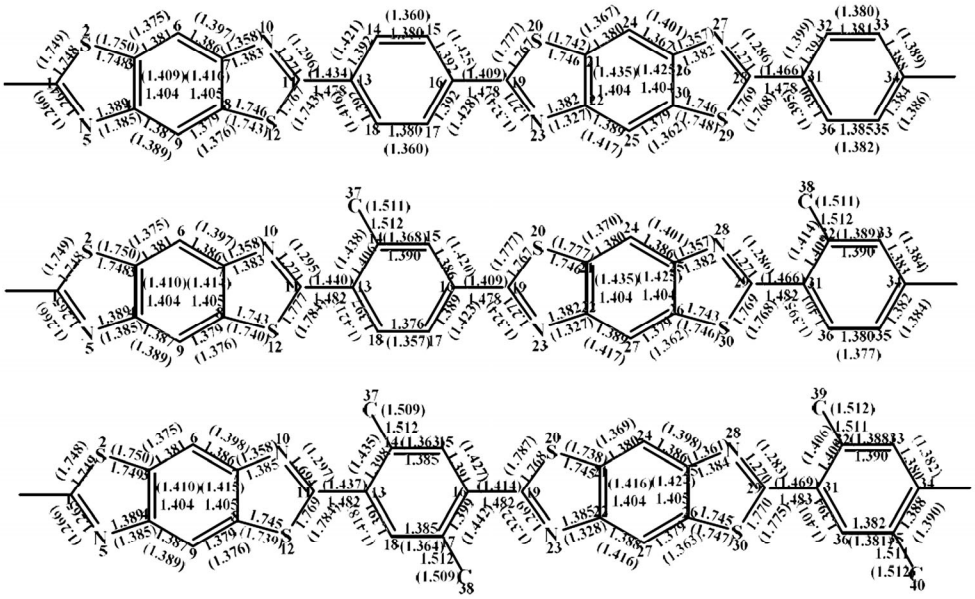

Fig. 6 — Comparison of the excited state geometries (values in parentheses) by CIS/6-31G(D) with the respected ground geometries using HF/6-31G(D) for $(PBZT)_2$, $(Me\text{-}PBZT)_2$, and $(di\text{-}Me\text{-}PBZT)_2$

tabulated in Table 4. Here also similar to the absorption spectra, the $S_1 \rightarrow S_0$ fluorescence peaks ($S_1 \rightarrow S_0$) have the strongest oscillator strengths in all the series, which arises exclusively from $\pi \rightarrow \pi*$ excitation and show the bathochromic shift depends on the substitution.

Reorganization energies

Namely, the band theory[36] and the hopping model[37] are widely used for describing the charge transport in organic materials. With the overlap of molecular orbitals of neighbouring molecules, the band is formed through which the conduction of the charge takes place according to the band theory model. On the other hand, the hopping model is more suitable where coupling between neighboring molecules are small, and this is more appropriate in our case here. Using this model the charge transport that is calculated here is the intermolecular process in which the charge hops between two molecules. The hole and electron transport process at the molecular level in the electroluminescent layer can then be portrayed as the electron transfer/hole transfer reactions between the neighbouring molecules[37].

$$M^{+/-} + M^{*} \rightarrow M^{*} + M^{+/-} \quad \ldots (1)$$

where **M*** is the neutral molecule interacting with neighbouring oxidized or reduced $\mathbf{M}^{+/-}$. In the case of electron transport, the interaction can be considered between a molecule in the neutral state interacting with a radical anion and in the case of hole transport the interaction can be considered between a molecule in the neutral state and a cation. The rate constant for electron transfer can be defined using the Marcus theory

$$K_{et} = \frac{4\pi^2}{h} \sqrt{\left(\frac{\pi}{\lambda_{\pm}} k_B T\right)}\, e^{-\lambda_{\pm}/4k_B T} \quad \ldots (2)$$

where ***t*** is the transfer integral/coupling matrix element between neighbouring molecules, $\lambda_{\pm}$ is reorganization energy, k_B is the Boltzmann constant and T the temperature. An evaluation of ***t*** would require the relative positions of the molecules in the solid-state as it is related to the energetic splitting of the frontier orbitals of the interacting molecules. On the other hand, the transports of the electron/hole are predictable from the reorganization energies and in general have good agreement with the experimental observations[21-24,38,39]. It is clear from the above that to have larger hole/electron transport; the reorganization energy of the corresponding change from neutral to cation/neutral to anion should be low. The reorganization energies are calculated based on the model as shown in Scheme 1 and this model has been applied with success in many earlier studies[21-24,38,39].

Here, λ_1 is the energy required for the reorganization of the neutral geometry to the cation

Table 4 — Electronic transitions data obtained by the TDDFT/B3LYP/6-31G(D) based on the CIS/6-31G(D) for all the oligomers

		Major contributions	λ_{max} (nm)	*Oscillator strength (f)*
PBZT	$S_0 \leftarrow S_1$	H→ L (80%)	314	0.7946
$(PBZT)_2$	$S_0 \leftarrow S_1$	H→ L (83%)	462	2.1376
$(PBZT)_3$	$S_0 \leftarrow S_1$	H→ L (98%)	478	3.5190
$(PBZT)_4$	$S_0 \leftarrow S_1$	H→ L (84%)	488	4.4287
Expt.			560[a]	
Me PBZT	$S_0 \leftarrow S_1$	H→ L (80%)	318	0.8200
$(Me\text{-}PBZT)_2$	$S_0 \leftarrow S_1$	H→ L (88%)	409	2.1625
$(Me\text{-}PBZT)_3$	$S_0 \leftarrow S_1$	H→ L (88%)	447	3.4122
$(Me\text{-}PBZT)_4$	$S_0 \leftarrow S_1$	H→ L (83%)	453	4.5643
di-Me-PBZT	$S_0 \leftarrow S_1$	H→ L (87%)	320	0.8009
$(di\text{-}Me\text{-}PBZT)_2$	$S_0 \leftarrow S_1$	H→ L (88%)	410	2.1397
$(di\text{-}Me\text{-}PBZT)_3$	$S_0 \leftarrow S_1$	H→ L (87%)	426	3.2512
$(di\text{-}Me\text{-}PBZT)_4$	$S_0 \leftarrow S_1$	H→ L (80%)	441	4.5060

[a] see ref. 33

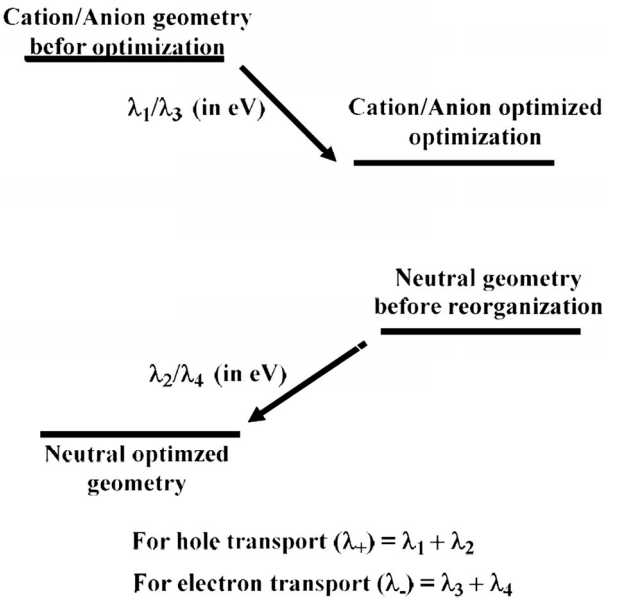

Scheme 1 — Calculation of reorganization energy

Table 5 — Reorganization energies (hole (λ_+)/electron (λ_-)) of monomers

Reorganization energies (eV)	Monomer		
	PBZT	Me-PBZT	di-Me-PBZT
λ_+	0.341	0.332	0.316
λ_-	0.301	0.305	0.300

geometry upon removal of an electron and λ_2, is the energy required to reorganize the obtained cation geometry back to a neutral state upon re-accepting an electron added up gives the total reorganization energy for the hole transport ($\lambda_+=\lambda_1+\lambda_2$) of the molecule when the charge is being transported. Similarly, the reorganization energy of the neutral to the anion (λ_3) and back (λ_4) should be useful in understanding the electron transport ($\lambda_-=\lambda_3+\lambda_4$). The reorganization energies for the hole transport (λ_+) and the electron transport (λ_-) for all the monomers are calculated and shown in Table 5. The reorganization energies for the hole transport in these monomers varies from 0.316-0.341 eV, which are higher than that of 4,4′-bis(phenyl-*m*-tolylamino) biphenyl (TPD) (λ_+=0.290 eV), which is a typical hole transport material[40]**.** The reorganization energies for the electron transport in these monomers varies from 0.300-0.305 eV, which are comparable to the tris (8-hydroxy-quinolinato) aluminum (III) (Alq3) (λ_-=0.276 eV), which a typical electron transport material[39]. In all these monmers it can be seen that the magnitude of λ_- is smaller than λ_+ (Table 5). From the reorganization energies point of view, these can be used as electron transport materials rather than the hole transport materials in LED devices.

Conclusions

Systematic investigations have been performed on the structural and electronic properties of some methyl substituted poly(*p*-phenylenebenzobisthiazole) oligomers are studied using DFT/B3LYP/6-31G(D) method. The conformational analysis has been carried out by the same methodology using the monomer unit of each oligomer. The frontier molecular orbital studies have shown that all the decisive molecular orbitals are delocalized on all subunits of the oligomers. The HOMO has an antibonding character between subunits, which may explain the nonplanarity observed for these oligomers in their ground state whereas the LUMO shows bonding character between the two adjacent rings, in agreement with the planar S_1 excited state. Excitation to the S_1 state corresponds to the promotion of an electron from the HOMO to the LUMO exclusively. The chain length dependence of IPs, EAs, $\Delta_{H\text{-}L}$s, and E_gs of the oligomers have been studied are found to be in good linearity. The extrapolation results of λ_{max} and HOMO-LUMO gap of unsubstituted PBZT are in good agreement with the experimental data. Generally, the absorption and emission spectra of these oligomers are red-shifted with the increase in the chain length. From the standpoint of reorganization energies, these can be used as the electron transport materials in LED devices. Thus, these theoretical methodologies help to understand the structure–properties relation of the conjugated materials and can be useful in designing new polymeric materials, which are useful in device applications.

Supplementary Data

Supplementary data associated with this article are available in the electronic form at http://nopr.niscair.res.in/jinfo/ijca/IJCA_60A(04)545-555_SupplData.pdf.

Acknowledgement

The author thanks to Dr K Bhanuprakash, CSIR-IICT, for his helpful discussions and also to KIM Division (IICT Comm. No. IICT/Pubs/2020/324) for their support.

References

1 Burroughes J H, Bradley D D C, Brown A R, Marks R N, Friend R H, Burn P L & Holmes A B, *Nature,* 347 (1990) 539.
2 Senevirathna M K I, Pitigala P K D D P & Tennakone K, *Phys Chem B,* 109 (2005) 16030.
3 Sirringhaus H, Brown P J, Friend R H, Nielsen M M, Bechgaard K, Langeveld-Voss B M W, Spiering A J H, Janssen R A J, Meijer E W, Herwig P & De Leeuw D M, *Nature*, 401 (1999) 685.
4 Friend R H, Gymer R W, Holmes A B, Burroughes J H, Marks R N, Taliani C, Bradley D D C, Dos Santos D A, Bredas J L, Logdlund M & Salaneck W R, *Nature,* 397 (1999) 121.
5 Kraft A, Grimsdale A C & Holmes A B, *Angew Chem Int Ed,* 37 (1998) 402.
6 Ranger M, Rondeau D & Leclerc M, *Macromolecules,* 30 (1997) 766.
7 Sriwichitkamol K, Surmaitr S, Poolmee P & Hannongbua S, *J Theor Comput Chem,* 5 (2006) 595.
8 Berggren M, Inganas O, Gustafsson G, Rasmusson J, Andersson M R, Hjertberg, T & Wennerstrom O, *Nature,* 372 (1994) 444.
9 Yang L, Feng J F, Ren A M & Sun J Z, *Polymer,* 47 (2005) 1397.
10 Yang W, Huang J, Liu C, Niu Y, Hou Q, Yang R & Cao Y, *Polymer,* 45 (2004) 865.

11 Sonar P, Zhang J, Grimsdale A C & Mullen K, *Macromolecules,* 37 (2004) 709.
12 Kumar S, *The Polymer Materials Encyclopedia*, Vol.10, Salamone J C (Ed), (CRC Press, Boca Raton) 1996.
13 Hearle J W S, *High-Performance Fibers*, (Wood head Publishing Ltd, Cambridge, UK) 2001.
14 Trohalaki, S & Dudis D, *Makromol Chem Macromol Symp,* 65 (1993) 163.
15 Prasad P N & Williams D J, *Introduction to Nonlinear Optical Effects in Molecules and Polymers*, (Wiley-Interscience, New York) 1991.
16 Bai S J, Wu C C, Tu L W & Lee K H, *J Polym Sci B:Polym Phys,* 40 (2002) 1760.
17 Bredas J L, Silbey R, Boudreaux D S & Chance R R, *J Am Chem Soc,*105 (1983) 6555.
18 Lahti P M, Obrzut J & Karasz F E, *Macromolecules,* 20 (1987) 2023.
19 Mushrush M, Facchetti A, Lefenfeld M, Katz H E & Marks T J, *J Am Chem Soc,* 125 (2003) 9414.
20 Zeng G, Yu W L, Chua S J & Huang W, *Macromolecules,* 35 (2002) 6907.
21 Yang L, Feng J K, Sun J Z, Ren A M & Sun C C, *Polymer,* 47 (2006) 3229.
22 Chidthong R, Hannongbua S, Aquino A J A, Wolschann P & Lischka H, *J Comput Chem,* 28 (2007) 1735.
23 Wang H, Wang X, Wang L, Wang H M & Liu A, *Int J Quantum Chem,* 107 (2007) 937.
24 Frisch M J *et al*, *Gaussian 09, Revision A.02*, (Gaussian Inc., Wallingford CT) 2009.
25 Yang Y & Welsh W J, *Macromolecules,* 23 (1990) 2410.
26 Trohalaki S & Dudis D S, *Polymer*, 36 (1995) 911.
27 Trohalaki S, Chabinyc M L, Resch T J, Fratini A V, Vance T A, Arnold F E & Dudis D S, *Chem Mater*, 8 (1996) 714.
28 Jenkins S, Jacob K I, Polk M B, Kumar S, Dang T D & Arnold F E, *Macromolecules,* 33 (2000) 8731.
29 Takahashi Y & Sul H, *J Polym Sci B: Polym Phys,* 38 (2000) 376.
30 Yang L, Liao Y, Feng J K & Ren A M, *J Phys Chem A*, 109 (2005) 7764.
31 Ford W K, Duke C B & Salaneck W R, *J Chem Phys*, 77 (1982) 5030.
32 Burrows P E, Shen Z, Bulovic V, McCarty D M, Forrest S R, Cronin J A & Thompson M E, *J Appl Phys,* 79 (1996) 7991.
33 Jenekhe S A, Osaheni J A. Meth J S & Vanherzeele H, *Chem Mater,* 4 (1992) 683.
34 Cai A, Sendt K & Reimers J R, *J Chem Phys,* 117 (2002) 5543.
35 Puschning P, Ambrosch D C, Heimel G, Zojer E, Resel R, Leising G, Kriechbaum M & Graupner W, *Synth Met,* 116 (2001) 327.
36 Marcus R & Sutin N, *Biochim Biophys Acta,* 811 (1985) 265.
37 Barbara P, Meyer T & Ratner M, *J Phys Chem,* 100 (1996) 13148.
38 Bredas J L, Beljonne D & Coropceanu V, Cornil, *Chem Rev,* 104 (2004) 4971.
39 Lin B C, Cheng C P, You Z Q & Hsu CP, *J Am Chem Soc,* 127 (2005) 66.
40 Gruhn N E, da Silva Filho D A, Bill T G, Malagoli M, Coropceanu V, Kahn A & Bredas J L, *J Am Chem Soc,* 124 (2002) 7918.